Intramolecular Charge-Transfer State Formation of 4-(*N*,*N*-Dimethylamino)benzonitrile in Acetonitrile Solution: RISM-SCF Study

Noriyuki Minezawa and Shigeki Kato*

Department of Chemistry, Graduate School of Science, Kyoto University, Kitashirakawa, Sakyo-ku, Kyoto 606-8502, Japan

Received: January 11, 2005; In Final Form: April 21, 2005

Intramolecular charge-transfer (ICT) state formation of 4-(*N*,*N*-dimethylamino)benzonitrile in acetonitrile solution is studied by the reference interaction site model self-consistent field (RISM-SCF) method. Geometry optimizations are performed for each electronic state in solution with the complete-active-space SCF wave functions. Dynamic electron correlation effects are taken into account by using the multiconfigurational quasidegenerate perturbation theory. Two-dimensional free energy surfaces are constructed as the function of the twisting and wagging angles of the dimethylamino group for the ground and locally excited (LE) states. The calculated absorption and fluorescence energies are in good agreement with experiments. The validity of the twisted ICT (TICT) model is confirmed in explaining the dual fluorescence, and the possibility of the planar ICT model is ruled out. To examine the mechanism of the TICT state formation, a "crossing" seam between the LE and charge-transfer (CT) state surfaces is determined. The inversion of two electronic states occurs at a relatively small twisting angle. The effect of solvent reorganization is also examined. It is concluded that the intramolecular twisting coordinate is more important than the solvent fluctuation for the TICT state formation, because the energy difference between the two states is minimally dependent on the solvent configuration.

1. Introduction

The formation of charge transfer (CT) states in solution is one of the fundamental processes in photochemistry. 4-(*N*,*N*-Dimethylamino)benzonitrile (DMABN) is a prototype of a class of organic donor−acceptor compounds which exhibit dual fluorescence in polar solvents.[1] The short-axis-polarized normal fluorescence (L_b type) band arises from a moderately polar locally excited (LE) state. The long-axis-polarized and red-shifted anomalous emission (L_a type) band has its origin in a strongly polar intramolecular charge transfer (ICT) state. Although DMABN and related donor−acceptor systems have been widely investigated,[2−4] the microscopic mechanism of the ICT formation reaction is still under controversy. Several models have been proposed to explain this unusual fluorescence behavior. They differ in the assumption of the reaction coordinate for the ICT process. The twisted ICT (TICT) model proposed by Grabowski et al.[5] has been generally accepted to be the origin of the L_a band. According to this model, a strong polar state is formed by 90° internal twisting of the dimethylamino group with respect to the benzene ring. The twisting motion is accompanied by charge transfer from the donor (dimethylamino group) to the acceptor (benzonitrile moiety). Zachariasse et al.[6] proposed an amino inversion mode as the source of charge separation. They suggested that a pyramidalization of the amino nitrogen induces a decoupling of the lone pair from the benzene ring and generates a large dipole moment. Later, they considered a planar quinoidal structure as a strong polar state.[7] In this planar ICT (PICT) model, the amino and benzonitrile moieties are strongly coupled, in contrast to the TICT model. Sobolewski et al.[8] proposed a cyano-bending model. A rehybridization of cyano carbon from linear sp toward bent sp^2 was discussed.

Recently, high-level ab initio calculations in the gas phase[8−14] have been carried out for DMABN. These calculations reproduce well the experimental data both in the gas phase and in nonpolar solvents, and most of them confirm the validity of the TICT model. However, the energy profile depends on the theoretical level. Some calculations employed the ground-state optimized geometry for all the electronic states, and the geometrical relaxation in the excited states was not taken into account. For energy calculations, both the static and dynamic electron correlation effects play an important role. The L_b state lies above the L_a state for all twisting angles at the configuration interaction singles (CIS) level, and the dynamic electron correlation, the $\sigma-\pi$ correlation in particular, leads to a drastic change in the energy profile of the CT state.[10]

Experimentally, the dual fluorescence of DMABN is observed neither under isolated molecule conditions nor in nonpolar solvents. Therefore, it would be insufficient to analyze the ICT reaction on the basis of the gas-phase energy profiles even if highly correlated methods are employed. Solvent effects are very important to understand the phenomena of dual fluorescence. Several calculations in solution phase[15−25] have been performed to obtain a clear understanding of the mechanism based on the TICT model. Statistical calculations such as Monte Carlo[15] and molecular dynamics (MD)[16,17] simulations for the solute−solvent systems have been carried out. In these simulation studies, however, the solute electronic structures were described on the basis of the calculations for the gas-phase DMABN molecule. Self-consistent reaction field (SCRF)[18,19] and polarizable continuum model (PCM)[20,21] calculations have also been performed. In these approaches, the solvation effects are directly incorporated in the solute electronic structures within the framework of the dielectric continuum model for solvents.[26]

10.1021/jp0580064 CCC: $30.25
Published on Web 05/28/2005

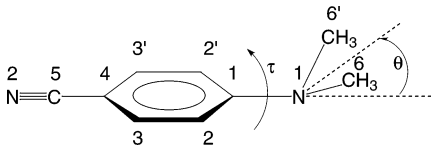

Figure 1. Coordinate system of DMABN.

In the present paper, we examine the TICT state formation of DMABN in acetonitrile solution by employing the reference interaction site model self-consistent field (RISM-SCF) method.[27,28] This method has been developed by combining ab initio electronic structure calculations of solute molecules with the RISM integral equation theory for solvents. The molecular aspects of the solvent are incorporated by site−site representation inherent in the RISM theory. By using this method, both the solute electronic and solvent structures are determined in a self-consistent manner with reasonable computational costs. The purpose of the present paper is to provide a realistic description of the free energy characteristic of DMABN in polar solvent. For this purpose, geometry optimizations are performed for solvated DMABN both in the ground and excited states by employing the complete active space (CAS) SCF method. The effects of dynamic electron correlation on the free energy profiles are estimated by the multiconfigurational quasidegenerate perturbation theory (MCQDPT).[29]

The organization of this paper is as follows. In section 2, details of the computational methods are presented. Section 3 describes the calculated results. Geometries and electronic properties of DMABN and solvation structures are discussed. Two-dimensional free-energy surfaces are constructed as the function of the twisting and wagging angles of the dimethylamino group for the ground and LE states. Absorption and fluorescence energies are calculated, and the results are compared with the available experimental data. In section 4, we discuss the mechanism of the TICT state formation in terms of the intramolecular twisting motion of DMABN and the solvent configuration. A "crossing" seam between the LE and CT state surfaces is determined by two-state MCQDPT calculations, and the barrier height is estimated. Finally, we examine the role of solvent motion in the TICT state formation. The conclusions are summarized in section 5.

2. Methods and Computational Details

Free-energy surfaces of DMABN in acetonitrile solvent were calculated as the functions of twisting and wagging angles of the dimethylamino group with respect to the benzonitrile plane (see Figure 1). The twisting angle τ was defined as the average of four dihedral angles: $C_2C_1N_1C_6$, $C_2C_1N_1C_6'$, $C_2'C_1N_1C_6$, and $C_2'C_1N_1C_6'$. The wagging angle θ was defined by C_1 bending out of the $N_1C_6C_6'$ plane.

We employed the RISM-SCF method[27,28] to calculate the free energies of the solvated DMABN, where the CASSCF wave functions were used to describe the solute electronic structures. The active space consists of nine orbitals, the π and π^* orbitals of the benzonitrile group and the amino nitrogen lone pair orbital, and ten electrons were distributed among them. The basis sets were the (9s5p1d)/[3s2p1d] set[30] for the C and N atoms and the (4s)/[2s] set[30] for the H atom, respectively. A set of diffuse p functions with the exponents of 0.034 and 0.048 for C and N[30] was added to each heavy atom in the benzonitrile moiety.

The RISM integral equation was solved with the hypernetted-chain (HNC) closure relation. For the solvent acetonitrile, we adopted the three-site model by Jorgensen and Briggs.[31] The temperature and density of the solution were fixed at 298.15 K and 0.777 g/cm^3, respectively. For the solute, the Lennard-Jones parameters were taken from the AMBER force field,[32,33] where all the H atoms were explicitly taken into account. The standard combination rule was applied to construct the solute−solvent van der Waals interaction potential.

Geometry optimizations were carried out at the RISM-CASSCF level. For the ground and LE states, the solute geometries were determined by optimizing the remaining degrees of freedom at given values of τ and θ. The twisting angle was varied between 0° and 90° with the step size of 15°, while we chose six values for the wagging angle θ: 0°, 5°, 15°, 30°, 45°, and 60°. For the CT state, the geometry optimizations were performed for the planar ($\tau = 0°$) and twisted ($\tau = 90°$) conformations. The optimization of this state at C_1 geometry failed because of the difficulty of convergence due to the root-flipping problem.

The dynamic electron correlation energies of the solute were estimated by the MCQDPT method, which is the second order for the CASSCF reference configurations. In the case of the RISM-SCF method, the correlated free energy is given by

$$\mathcal{A} = \langle \Psi^{\mathrm{SCF}} | \hat{H}_0 | \Psi^{\mathrm{SCF}} \rangle + E^{(2)} + \Delta\mu^{\mathrm{SCF}} \qquad (1)$$

where $\hat{H}_0$ is the electronic Hamiltonian in the gas phase, $E^{(2)}$ is the correlation energy, and $\Delta\mu^{\mathrm{SCF}}$ is the excess chemical potential obtained by the RISM-SCF method. It is noteworthy that the solvated Fock operator was used in constructing the zeroth-order Hamiltonian for the perturbation calculations instead of the usual gas-phase Fock operator. With this modification, we can include the change of excess chemical potential due to the first-order wave function as discussed in the Appendix.

We carried out MCQDPT[29] calculations at the CASSCF optimized geometries and constructed the two-dimensional (τ, θ) free-energy surfaces. The RISM-CASSCF wave function was adopted as the zeroth-order one, and the carbon and nitrogen 1s electrons were kept frozen in the perturbation calculations. The intruder state avoidance method was employed with the energy denominator shift parameter of 0.02.[34]

Besides the calculations in solution, we performed CASSCF and MCQDPT calculations of DMABN in the gas phase in order to evaluate the solvation effect.

3. Free-Energy Surfaces

3.1. Ground State. Ground-state geometries at the MCQDPT minimum energies are shown in Table 1. A pyramidal structure was obtained both in the gas and solution phases. In the gas phase, the optimized structure is in good agreement with previous calculations[9,12] as well as with the X-ray crystal structure.[35] The wagging angle θ strongly depends on the theoretical level. It is calculated to be 28.2° in the gas phase, which is larger than the experimental value of 11.9° for the crystal. As a result, the calculated C_1-N_1 bond length, 1.397 Å, is slightly longer than the crystal structure value of 1.365 Å because of the decrease of conjugation between the amino lone pair and benzene π orbitals. In the solution phase, the optimized geometrical parameters are very similar to those in the gas phase. The difference from the gas-phase bond distances is within 0.01 Å. Cammi et al.[21] observed the same trend in their PCM calculations. When compared with their geometry optimized by DFT combined with the PCM approach, the C_1N_1 and C_4C_5 bond lengths increase by 0.02 Å while the C_5N_2 bond length

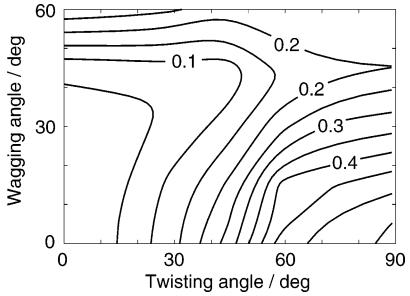

Figure 2. Two-dimensional HNC free-energy surface for the ground state of DMABN. Energy (in eV) is measured from the minimum (0° twisting and 28° wagging). Contour spacing is 0.05 eV.

TABLE 1: Optimized Geometries for the Ground (S_0), LE, PICT, and TICT States[a]

	S_0	LE	PICT	TICT
τ/deg	0	0	0	90
		Gas		
symmetry	C_s	C_{2v}	C_{2v}	C_{2v}
C_1N_1	1.397	1.372	1.397	1.436
C_1C_2	1.413	1.439	1.438	1.430
C_2C_3	1.394	1.433	1.387	1.374
C_3C_4	1.400	1.434	1.446	1.438
C_4C_5	1.447	1.432	1.412	1.422
C_5N_2	1.150	1.153	1.161	1.157
N_1C_6	1.452	1.451	1.454	1.460
θ	28.2	0.0	0.0	0.0
		Solution		
symmetry	C_s	C_{2v}	C_{2v}	C_{2v}
C_1N_1	1.389	1.368	1.407	1.438
C_1C_2	1.413	1.439	1.427	1.424
C_2C_3	1.392	1.434	1.394	1.375
C_3C_4	1.400	1.425	1.445	1.442
C_4C_5	1.445	1.436	1.408	1.412
C_5N_2	1.150	1.152	1.165	1.161
N_1C_6	1.452	1.454	1.451	1.459
θ	27.7	0.0	0.0	0.0

[a] Bond lengths in angstroms and angles in degrees.

decreases by 0.02 Å. Since these differences are already found in the gas phase, they are attributed to the methods of the electronic structure calculations for the solute rather than the treatment of the solvation effects.

The two-dimensional (τ, θ) free-energy surface for the ground state is shown in Figure 2. A qualitatively similar free-energy profile is obtained at the RISM-CASSCF level. The surface is that of a double well for the wagging angle, although a very flat region is observed for small twisting angles. The wagging angle at the minimum free-energy point is calculated to be 27.7°. The geometrical parameters at this point are shown in Table 1. The inversion barrier of the dimethylamino group is 0.2 kcal/mol at $\tau = 0°$ and increases along the twisting angle, and it finally reaches 8.4 kcal/mol at $\tau = 90°$. In Figure 3, the free-energy curves along the twisting coordinate are shown. The minimum free-energy point for each τ is chosen from the corresponding two-dimensional (τ, θ) data. For comparison, the potential energy curve calculated along the gas-phase minimum-energy path is also shown. As seen in the figures, the ground-state energy gradually increases with the twisting angle and reaches the maximum at $\tau = 90°$ both in the gas phase and in solution. The barrier heights for the amino−phenyl internal rotation were calculated to be 2.6 and 4.6 kcal/mol in the gas phase and in solution, respectively. To estimate the zero-point energy (ZPE) effect on the barrier heights, we carried out

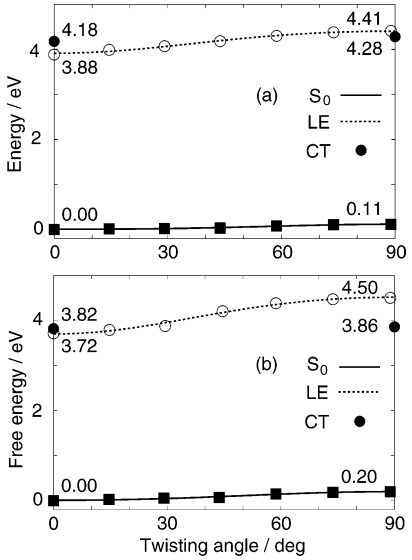

Figure 3. Profiles of (a) gas-phase potential energy and (b) solution-phase HNC free energy along the twisting coordinate. Note that only two points are available for the CT state because of a root flipping problem.

TABLE 2: Solvation Free Energies and Solute−Solvent Interaction Energies for DMABN[a]

	τ/deg	$\Delta\mu^{HNC}$	$\Delta\mu^{GF}$	E_{int}	$(E_{es})^b$
S_0	0	16.0	−12.8	−30.7	(−9.1)
	90	17.8	−11.6	−28.4	(−7.2)
LE	0	15.0	−14.3	−32.7	(−11.0)
	90	18.2	−11.3	−28.1	(−7.0)
PICT	0	4.6	−27.5	−53.1	(−31.9)
TICT	90	1.8	−33.0	−60.3	(−40.0)

[a] Unit: kcal/mol. [b] Electrostatic interaction.

vibrational analyses at the CASSCF level in the gas phase.[36] The barrier heights were slightly reduced to 1.8 and 3.9 kcal/mol in the gas phase and in solution, respectively. Experimentally, the ground-state rotation barrier was estimated to be 7.6 kcal/mol.[37]

To examine the solvation effects, the average solute−solvent interaction energies and solvation free energies are summarized in Table 2. The former is given by

$$E_{\mathrm{int}} = \sum_{\alpha,s} \langle u_{\alpha s} \rangle = \rho \sum_{\alpha,s} \int \mathrm{d}\mathbf{r}\, g_{\alpha s}(r)\, u_{\alpha s}(r) \qquad (2)$$

where the Greek subscripts refer to the solute sites and the Roman refer to the solvent sites. ρ is the number density of the solvent, and $g_{\alpha s}$ represents the site−site radial distribution functions (RDFs). The solvation free energy is obtained by two expressions. The first column ($\Delta\mu^{HNC}$) is derived from the HNC closure[38]

$$\Delta\mu^{\mathrm{HNC}} = -\frac{\rho}{\beta} \sum_{\alpha,s} \int \mathrm{d}\mathbf{r} \left(c_{\alpha s} + \frac{1}{2} h_{\alpha s} c_{\alpha s} - \frac{1}{2} h_{\alpha s}^{\,2} \right) \qquad (3)$$

and the second ($\Delta\mu^{GF}$) from an assumption of Gaussian fluctuations[39]

$$\Delta\mu^{\mathrm{GF}} = -\frac{\rho}{\beta} \sum_{\alpha,s} \int \mathrm{d}\mathbf{r} \left(c_{\alpha s} + \frac{1}{2} h_{\alpha s} c_{\alpha s} \right) \qquad (4)$$

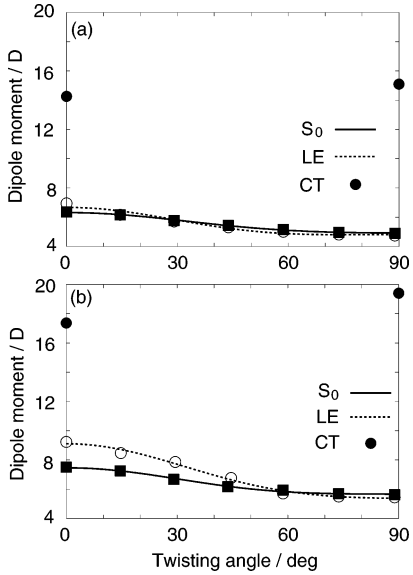

Figure 4. Profiles of dipole moments along the twisting coordinate (a) in gas phase and (b) in solution. Note that only two points are available for the CT state because of a root flipping problem.

TABLE 3: LSF Partial Charges and Dipole Moments

	τ/deg	NMe_2	(N_1)	Bz	CN	(N_2)	dipole/D
			Gas				
S_0	0	−0.11	(−0.38)	0.23	−0.12	(−0.47)	6.36
	90	−0.23	(−0.41)	0.34	−0.11	(−0.46)	4.90
LE	0	0.08	(−0.13)	0.07	−0.15	(−0.45)	6.94
	90	−0.28	(−0.47)	0.42	−0.14	(−0.44)	4.74
PICT	0	0.31	(0.02)	−0.11	−0.20	(−0.58)	14.26
TICT	90	0.63	(0.34)	−0.40	−0.22	(−0.54)	15.10
			Solution				
S_0	0	−0.10	(−0.38)	0.22	−0.11	(−0.55)	7.50
	90	−0.23	(−0.43)	0.35	−0.11	(−0.53)	5.63
LE	0	0.16	(−0.02)	−0.02	−0.15	(−0.51)	9.24
	90	−0.28	(−0.48)	0.43	−0.15	(−0.51)	5.44
PICT	0	0.37	(0.05)	−0.12	−0.26	(−0.68)	17.22
TICT	90	0.68	(0.34)	−0.43	−0.25	(−0.66)	19.19

where $c_{\alpha s}$ and $h_{\alpha s}$ are the direct and total correlation functions, respectively. The GF expression can be derived by assuming that the solvent perturbs in a linear response manner to the solute molecule. As shown in Table 2, the solute−solvent interaction energy is decreased by 2.3 kcal/mol along the twisting motion. This is mainly due to a decrease in the solute−solvent electrostatic interaction, which is estimated to be 1.9 kcal/mol, and the Lennard-Jones interaction is nearly constant.

Dipole moments of DMABN along the twisting coordinate are shown in Figure 4. They are derived from the partial charges which are determined at the CASSCF level by least-squares fitting to the electrostatic potential. In Table 3, the dipole moments and partial charges at some important points are summarized. At $\tau = 0°$, the dipole moments are calculated to be 6.36 and 7.50 D in the gas phase and in solution, respectively. The values in solution are slightly larger than those in the gas phase because of the electronic polarization induced by polar solvent. The present calculations effectively reproduce the experimental value of 6.6 D in 1,4-dioxane.[6] The dipole moments for the ground state decrease along the twisting coordinate both in the gas phase and in solution. At the same time, the partial charges of the donor group become more negative. These are due to a decrease of the overlap between the donor and acceptor orbitals. A decrease in dipole moments along the wagging angle is also observed, although it is small compared with the twisting motion.

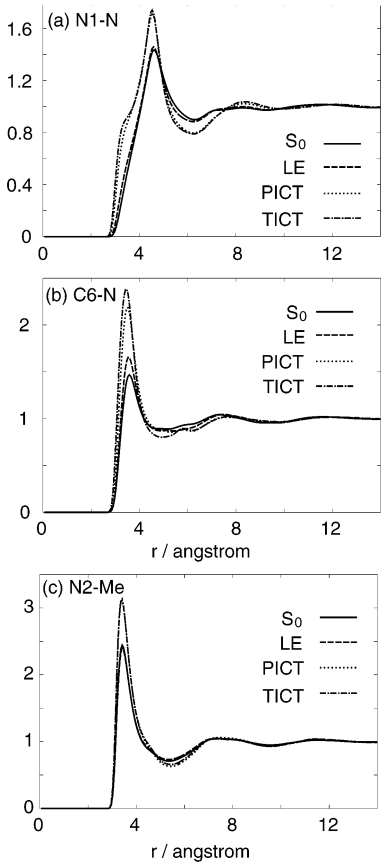

Figure 5. Site−site radial distribution functions between the solute and solvent sites in acetonitrile. (a) N_1−N, (b) C_6−N, and (c) N_2−Me.

TABLE 4: Absorption and Fluorescence Energies (in eV) in Gas Phase and in Acetonitrile Solvent

	absorption		fluorescence	
	LE	CT	L_b	L_a
	Gas			
MCQDPT	4.20	4.49	3.80	3.54
exptl[a]	4.25	4.56		
	Solution			
RISM-MCQDPT	4.18	4.34	3.49	2.60
exptl[b]		4.26	∼3.4	∼2.6

[a] Reference 40. [b] References 41 and 42.

The RDFs are shown in Figure 5. We confine our attention to N_1 and C_6 atoms in the donor dimethylamino group and the N_2 atom in the acceptor cyano group. The N_1−N distribution function shows a broad first peak at 4.5 Å. Since the N_1 atom is negatively charged (−0.38), this peak results from the interaction between neighboring sites and solvent N. For the C_6−N distribution function, a sharp peak is observed at 3.5 Å. This means that the solvent acetonitrile molecules around the donor group are mainly coordinated to the positively charged (+0.14) methyl groups. For the N_2−Me distribution function, a marked peak is observed at 3.5 Å, which is attributed to the electrostatic interaction with the negatively charged N_2 atom (−0.54).

Absorption energies for DMABN are summarized in Table 4. For comparison, experimental data are also included. To estimate the absorption energies, we assumed that the electronic transition to the final state is fast enough to leave the solute geometry and the solvation structure frozen at the ground state (vertical transition). Thus, the energies of the ground and excited

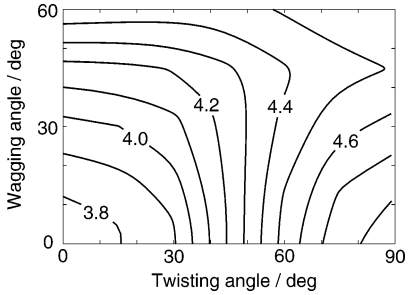

Figure 6. Two-dimensional HNC free-energy surface for the LE state of DMABN. Energy (in eV) is measured from the ground-state minimum (0° twisting and 28° wagging). Contour spacing is 0.1 eV.

states were calculated with the Hamiltonian

$$\hat{H} = \hat{H}_0 + \sum_{\alpha} \hat{Q}_{\alpha} V_{\alpha} \tag{5}$$

where $\hat{Q}_{\alpha}$ is the population operator and V_{α} is the electrostatic potential acting on the solute site α which is generated from the solvent distribution equilibrium to the ground-state solute charge distribution, respectively. We adopted the ground-state geometry given in Table 1. In the gas phase, MCQDPT excitation energies of 4.20 and 4.49 eV are computed for the LE and CT states, respectively. These values are in good agreement with the experimental data[40] of 4.25 and 4.56 eV. The first excited state has *B* symmetry and is only a weakly allowed transition (the computed oscillator strength is very small[8,9,11,13,14]). The strong absorption is assigned as the transition to the second excited state with *A* symmetry. In solution, a strongly polar CT state is stabilized effectively by polar solvent. Computed excitation energies are 4.18 and 4.34 eV. The calculated transition energy to CT, 4.34 eV, is in good agreement with the experimental value[41] of 4.26 eV. Compared with the gas-phase result, the excitation energy to the CT state is red-shifted by 0.15 eV.

3.2. LE State. The LE state geometries corresponding to the minima for the MCQDPT surfaces are shown in Table 1. A planar C_{2v} structure was obtained both for gas and solution phases. In the solution phase, we obtained two conformations with C_{2v} symmetry. These are the results of optimizations with different configurations of the methyl groups. The free-energy difference between them is 1.1 kcal/mol, and the lower-energy conformation is shown. No experimental data are available for this state, but the optimized structure is in qualitative agreement with previous computational results.[12] The C_1C_2, C_2C_3, and C_3C_4 bond lengths are much longer than those of the ground state. This is because the LE state is characterized by the HOMO $\rightarrow$ LUMO + 1 and HOMO − 1 $\rightarrow$ LUMO single excitations. These configurations are described mainly by $\pi \rightarrow \pi^*$ in the benzene ring. The wagging angle θ is equal to 0.0°, while that of the ground-state value is 28.2°. The coupling of the donor and acceptor groups is enhanced in the planar structure. Consequently, the C_1N_1 bond shrinks and shows some double-bond character. In the solution phase, the geometrical parameters are very similar to those in the gas phase. The difference is less than 0.01 Å.

The two-dimensional (τ, θ) free-energy surface for the LE state is shown in Figure 6. The minimum free-energy point is located at (0°, 0°). This surface has a double well at the region $\tau > 50°$. The inversion barriers of the dimethylamino group are 3.3 and 8.0 kcal/mol at $\tau = 60°$ and 90°, respectively. As shown in Figure 3, DMABN is destabilized along the twisting angle both in the gas phase and in solution. In the gas phase, the barrier heights for the internal rotation around the amino−phenyl bond are calculated to be 12.2 and 12.1 kcal/mol with and without the ZPE correction, which is larger than the ground-state value by 10.4 kcal/mol. In solution, the twisting barrier increases to 17.8 kcal/mol including the ZPE correction and is higher in energy than that of the ground state by 13.9 kcal/mol.

As shown in Table 2, the solute−solvent interaction energy decreases by 4.6 kcal/mol along the twisting coordinate. A decrease in the electrostatic part is calculated to be 4.0 kcal/mol, and the Lennard-Jones part changes very little. The dipole moments of the LE state are shown in Figure 4 and Table 3. For $\tau = 0°$, they are calculated to be 6.94 and 9.24 D in the gas phase and in solution, respectively. As seen in Figure 4, the dipole moment decreases along the twisting angle and becomes the minimum at $\tau = 90°$. This is an origin of the enhancement of the twisting barrier in solution.

RDFs for the LE state are shown in Figure 5. For the C_6−N distribution, the first peak slightly increases compared with the ground state, while the N_2−Me distribution is very similar to the ground state. This is because the partial charge of −0.51 is almost the same as −0.54 in the ground state.

The L_b fluorescence energies corresponding to emission from the LE state are shown in Table 4. We employed the geometries of the LE state given in Table 1 and adopted the solvation structure for the LE state obtained by the RISM-CASSCF method. The computed value in solution is 3.49 eV, which is in good agreement with experiments[41,42] (∼3.4 eV). The L_b band is slightly red-shifted (∼0.3 eV) because of the solvation.

3.3. CT State. Because of a root flipping problem in the CASSCF iteration process, we could obtain the optimized geometries of the CT state only at $\tau = 0°$ and 90°. The resultant geometric parameters are summarized in Table 1. At $\tau = 0°$, a planar C_{2v} conformation (PICT) was obtained both in the gas and solution phases. The wave function is mainly composed of the HOMO $\rightarrow$ LUMO excitation, though the HOMO orbital mixes strongly with the amino lone-pair orbital. In the gas phase, a quinoidal structure is observed. The single bonds alternate with the double bonds in the benzonitrile moiety. In the solution phase, the C_1N_1 bond becomes longer, indicating that the amino lone-pair orbital is decoupled from the π orbitals of the benzonitrile moiety because of the strong solvation even at the planar conformation. As a result, a quinoidal structure is suppressed. This is because the donor and acceptor groups are solvated individually, and a large electronic polarization occurs. At the twisted conformation (TICT), the wave function is fully characterized by the amino n $\rightarrow$ LUMO excitation. The optimized geometry has C_{2v} symmetry, and the benzonitrile moiety has a quinoidal character. On the contrary to the case of $\tau = 0°$, the optimized geometry changes very little in passing from vacuum to solution. Note that in PCM calculations[21] the C_1N_1 bond length is much shorter than the present results both at $\tau = 0°$ and 90°.

Experimentally, the endothermicity for the formation of TICT state in the gas phase and in nonpolar solvent is well-established, because no anomalous emission at a longer wavelength region is observed under such conditions. Polimeno et al.[25] estimated that the TICT state energy is located above the LE state by 11.5 kcal/mol by extrapolating experimental data with various solvents. The present calculations provide a comparable value for the energy difference between the two states in the gas phase: 8.9 kcal/mol with the ZPE correction of −0.3 kcal/mol. In polar solvents, the CT state is stabilized and the TICT state formation process is considered to become exothermic. The reaction free energy ΔG is estimated to be −2.8 kcal/mol in

acetonitrile from time-resolved fluorescence spectroscopy experiments[43] with the aid of kinetic equation analyses. As seen in Figure 3, the PICT state free energy is higher than that of the LE state by 2.3 kcal/mol, and the free energy difference between the TICT and LE states is estimated to be 3.2 kcal/mol in the present calculations. If we adopt the GF free energy difference between the LE and TICT states, the reaction free energy ΔF becomes -2.1 kcal/mol, indicating that the TICT state formation is exothermic. Note that the present free energy is not Gibbs energy but Helmholtz.

As shown in Figure 4 and Table 3, the dipole moment for the CT state is already large at $\tau = 0°$. Computed dipole moments are 14.3 and 17.2 D in the gas phase and in solution, respectively. At the TICT state, they become 15.1 and 19.2 D. In experiments, the CT state dipole moment is estimated to be 13−20 D, which is consistent with the present results. The partial charge of the donor group has a large positive value, and a charge of about 0.3−0.4 is transferred to the acceptor and distributes all over the benzonitrile moiety by the conformational change to the TICT state.

Remarkable changes in RDFs are observed for the two CT state conformations compared with the ground and LE states as shown in Figure 5. For the N_1-N distributions, the height of the first peak increases, and a weak shoulder appears around 3 Å. The former is expected, because the N_1 atom has a positive charge of 0.05 (CT) and 0.34 (TICT). The shoulder indicates that the solvent N atom approaches the solute N_1 atom perpendicularly with respect to the $N_1C_6C_6'$ plane. The distance of 3 Å is nearly equal to the sum of the core radii for solute N_1 and solvent N atoms. Since the donor group is planar, it is easy for solvent molecules to approach the inner N_1 atom. The more positive N_1 charge in the TICT state causes a shift of the shoulder to the inner region. For the C_6-N distributions, a rather sharp first peak is observed at 3.5 Å. The methyl group has a slightly positive charge of 0.16 (CT) and 0.17 (TICT). It serves as an electron-donating group stabilizing the N_1 atom by its induction effect and hyperconjugation. For the N_2-Me distributions, a large increase in the first peak is observed for the two CT state conformations, because the N_2 atom has a larger negative charge of -0.68 (PICT) and -0.66 (TICT).

The relative stability between the PICT ($\tau = 0°$) and TICT ($\tau = 90°$) states has been a matter of discussion in specifying the emitting state.[44] In the gas phase, the energy of the TICT state is higher than that of PICT by 2.2 kcal/mol, as seen in Figure 3. The ZPE corrections reduced the energy difference to only 0.2 kcal/mol. Both the CT states are strongly stabilized because of the solvation, and the dipole moments are enhanced by 3.0 and 4.1 D for the $\tau = 0°$ and 90° conformers, respectively. Despite stronger solvation for TICT, the free energy of TICT is still higher than that of PICT by 0.9 kcal/mol, even in polar acetonitrile solvent. We tabulated the excess chemical potentials obtained by the HNC and GF approximations in Table 2. As seen here, the values of $\Delta\mu^{HNC}$ remain positive despite large solute−solvent electrostatic stabilization for the CT states. This is attributed to an overestimation of the solvent cavity formation energy inherent in the RISM theory. Since a twisting of the dimethylamino group modifies the cavity shape and size, this drawback may cause some error in estimating the difference of excess chemical potential between the two conformers. On the other hand, the GF approximation provides negative values of the excess chemical potential. If we use the GF excess chemical potential $\Delta\mu^{GF}$ in place of $\Delta\mu^{HNC}$, the TICT free energy becomes lower than that of PICT by 2.0 and 1.8 kcal/mol with and without the ZPE correction. Note that we used the gas-phase ZPE values for the CT states. However, it is noted that the free energy defined in this way is not self-consistent with the solute electronic wave function, because $\Delta\mu^{GF}$ does not satisfy the variational condition. In summary, both the PICT and TICT paths are possible for the ICT formation in terms of free energy. So, we calculate emission energies with geometries for the two CT states and compare them with available experimental data.

The L_a fluorescence energies are summarized in Table 4. We used the optimized geometries for the PICT and TICT states given in Table 1 and the solvent structure for each CT state in calculating the fluorescence energies. In solution, the PICT and TICT emission energies are calculated to be 3.65 and 2.60 eV, respectively. Although the PICT state free energy is lower than that of the TICT one by 0.9 kcal/mol (0.04 eV), its emission energy is much larger by 1.1 eV. Experimentally, a broad peak around 2.6 eV is observed.[41,42] The calculated TICT emission energy quantitatively reproduces the experimental value, while a large deviation is observed for the PICT emission. In the latter case, the calculated L_a band is blue-shifted even from the L_b normal band. The same calculations in the gas phase give 4.13 and 3.54 eV for the PICT and TICT emissions. Therefore, the large PICT emission energy is attributed to the relatively stable ground state at the PICT state geometry, not to the solvation effect. From the present calculations, the TICT model is concluded to be the origin of the anomalous emission band. It is noted that this result does not change even if the ZPE corrections are included, because the difference in the ZPE between the electronic states is at most 0.1 eV.

4. Mechanism of TICT State Formation

4.1. Surface Crossing. The initial photoabsorption is attributed to the transition to the CT state because of its large transition moment. After the excitation, the relaxation of solute geometry and solvent distribution around the solute can occur. Although the CT state energy is 3.7 kcal/mol higher than the LE energy at the vertically excited point, the CT energy becomes slightly lower than the LE, 0.7 kcal/mol at the equilibrium geometry of the CT state at $\tau = 0°$. We can therefore expect that the nonadiabatic transition occurs to the LE state during the relaxation process through a surface crossing between the two states.

At the minimum free-energy point of the LE state, the CT state is located at 0.47 eV in energy above the LE state. To proceed with the TICT formation reaction from the LE state, the nonadiabatic crossing or avoided crossing point between the two surfaces is required. We calculate the energy difference between the LE and CT states as the function of the two angles θ and τ to locate the region where the nonadiabatic transition can effectively occur. The MCQDPT calculations based on the 1:1 state-averaged (SA) CASSCF for these two states were carried out at 36 points of the (τ, θ) pair to treat these two states equivalently. We employed the solute geometry and electrostatic potentials acting on the solute atomic sites optimized for the LE state at each (τ, θ) point. The results are shown in Figure 7. Although the two surfaces show avoided crossing because these belong to the same symmetry except at $\tau = 0°$ and 90°, the magnitude of avoided crossing was found to be considerably small. We therefore plotted the zero-energy-difference line in Figure 7. The solute electronic energies for the two states are inverted at $\tau = 30°$. Note that the solvent molecules are in equilibrium with the LE state for every (τ, θ) point. When DMABN follows the minimum free-energy path for the LE state, a "crossing" occurs near at (28°, 28°). The free energy increases

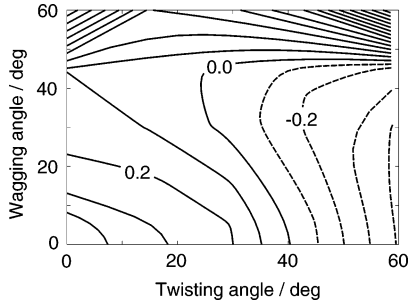

Figure 7. Energy difference between the LE and CT states. Contour spacing is 0.1 eV. Solid line means positive (CT > LE) and dashed line negative (CT < LE).

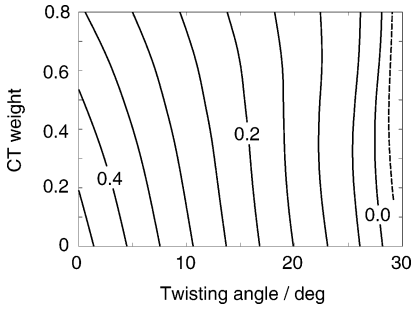

Figure 8. Energy difference between the LE and CT states as the function of the twisting angle τ and solvation coordinate w. Contour spacing is 0.05 eV. Solid line means positive (CT > LE) and dashed line negative (CT < LE).

by 7.3 kcal/mol from the LE minimum (0°, 0°). Hicks et al. have estimated the reaction barrier in butyronitrile as 3.2 ± 0.8 kcal/mol.[45] Although butyronitrile is more polar than acetonitrile, the present calculations seem to overestimate the reaction barrier.

4.2. Nonequilibrium Solvation. For many electron-transfer reactions, the nonequilibrium solvation effect plays an important role in determining the activation energies. We examine here such an effect in the present TICT state formation process. First, SA RISM-CASSCF calculations of the LE and CT states were performed with varying weights of the CT state w from 0 to 1. From these calculations, we obtained the solvent distributions, which are in equilibrium with the weighted solute charge distributions and thus the electrostatic potentials acting on the solute atomic sites, $\mathbf{V}(\tau, \theta, w)$, as the function of the CT state weight w as well as the geometric parameters θ and τ. We used the optimized geometries for the LE state as in section 4.1. Next, two-state 1:1 MCQDPT calculations were carried out under the influence of electrostatic potential $\mathbf{V}(\tau, \theta, w)$ at each point of (τ, θ), and the energies of LE and CT states were obtained. Note that the energy difference map in Figure 7 corresponds to the case of $w = 0$ (i.e., equilibrium with the LE state charge distributions).

We show the change of energy difference as the function of twisting angle τ and the solvation coordinate w in Figure 8. The wagging angle θ was determined along the minimum free-energy path for the LE state, Figure 6. Because of a root flipping problem, the SA RISM-CASSCF calculations were performed with the weight in the range from 0 to 0.8 for $\tau \neq 0°$. At the planar conformation $\tau = 0°$, the energy gap between the LE and CT states monotonically decreases with increasing w, 0.47 eV for $w = 0$ and 0.32 eV for $w = 1$, respectively. However, it becomes almost constant along w at $\tau > 20°$, as seen in Figure 8. Although it is possible for the solvent to rearrange prior to the twisting motion, the "crossing" is not achieved by the nonequilibrium solvation effect but by the intramolecular twisting motion. This is in contrast to typical electron-transfer reactions, where the solute charge distribution between the initial and final states and thus solvent reorientation becomes crucial in proceeding the reaction. In the present DMABN system, the initial LE state is already moderately polar, and the direction of dipole moments is the same between the two states. In such a case, the change of solvent distribution stabilizing one state also stabilizes the other state.

Fonseca et al.[22] and Kim and Hynes[23] constructed the two-dimensional free-energy surface and found that the barrier is formed along the intramolecular twisting barrier. In dynamics relevant to the barrier crossing, both the intramolecular twisting and solvent motions were found to play an important role.

It should be noted that we employed the LE state optimized geometries in the present calculations. The geometrical change of DMABN also occurs for the TICT state formation process, and thus, the present calculations may give an upper limit of the reaction barrier.

5. Concluding Remarks

In this study, the ICT state formation of DMABN in acetonitrile solution was studied by the RISM-SCF method. Dynamic electron correlation effects were taken into account by the MCQDPT method. Two-dimensional free-energy surfaces as the function of the twisting and wagging angles were constructed for the ground and LE states. The calculated absorption and fluorescence energies are in good agreement with experiments. The validity of the TICT model is confirmed in explaination of the dual fluorescence. The PICT model is ruled out, because its emission energy is considerably larger than the experimental value. A "crossing" seam between the LE and CT state surfaces was determined by two-state MCQDPT calculations. It is found that the inversion of two electronic states occurs at a relatively small twisting angle (~30°). To examine the role of solvent motion in the TICT state formation, the solute electronic energy difference map was constructed as the function of the twisting angle and the solvation coordinate. The energy difference between the two states was minimally dependent on the solvent configuration and is mainly affected by the twisting motion. This is in contrast to typical electron-transfer reactions. In the present DMABN system, the intramolecular twisting motion is more important than the solvent fluctuation because the LE and CT states have the same direction of the dipole moment.

Acknowledgment. This work was supported by a Grant-in-Aid from the Ministry of Education and Science, Japan.

Appendix

In MCQDPT calculations, we adopt site potentials and solvation free energies optimized by the RISM-CASSCF method. It appears that the solute electronic energy at the MCQDPT level and the excess chemical potential obtained by the RISM-CASSCF method are inconsistent. However, we can include the change of excess chemical potential due to the first-order wave function of the solute molecule. For the excess chemical potential, we adopt the free energy derived from the HNC closure relation by Singer and Chandler[38] (see eq 3). The first-order wave function modifies solute partial charges, and the change of excess chemical potential is given by

$$\Delta\mu = \Delta\mu^{\mathrm{HNC}} + \sum_{\gamma} \frac{\partial \Delta\mu^{\mathrm{HNC}}}{\partial Q_{\gamma}} \Delta Q_{\gamma} \qquad \text{(A1)}$$

The first derivative of the excess chemical potential with respect to the site charge Q_γ is written as

$$\frac{\partial \Delta\mu^{\mathrm{HNC}}}{\partial Q_\gamma} = -\frac{\rho}{\beta}\sum_{\alpha s}\int \mathrm{d}\mathbf{r}\left[\{\text{HNC equation}\}\frac{\partial t_{\alpha s}}{\partial Q_\gamma} + \{\text{definition of } t\}\frac{\partial h_{\alpha s}}{\partial Q_\gamma} + \{\text{RISM equation}\}\frac{\partial c_{\alpha s}}{\partial Q_\gamma}\right] + \rho\sum_{\alpha s}\int \mathrm{d}\mathbf{r}\, \mathrm{e}^{-\beta u_{\alpha s}+t_{\alpha s}}\frac{\partial u_{\alpha s}}{\partial Q_\gamma} \quad \text{(A2)}$$

where $t_{\alpha s} = h_{\alpha s} - c_{\alpha s}$. By using the variational conditions of excess chemical potentials,[28,38] the curly bracket terms vanish. The last term, which includes the derivative of the solute−solvent interaction potentials $u_{\alpha s}(r)$, is reduced to

$$\rho\sum_{\alpha s}\int \mathrm{d}\mathbf{r}\, g_{\alpha s}(r)\frac{Q_s\delta_{\alpha\gamma}}{r} = \rho\sum_{s} Q_s\int \mathrm{d}\mathbf{r}\,\frac{g_{\gamma s}(r)}{r} = V_\gamma \quad \text{(A3)}$$

As a result, the change of excess chemical potential is given by

$$\Delta\mu = \Delta\mu^{\mathrm{HNC}} + \sum_\alpha \Delta Q_\alpha V_\alpha \quad \text{(A4)}$$

The second term corresponds to the change of solute−solvent electrostatic interaction caused by the solute charge modification. The total Hamiltonian is defined by $\hat{H} = \hat{H}_0 + \sum_\alpha \hat{Q}_\alpha V_\alpha$. When the zeroth-order Hamiltonian is constructed by the solvated Fock operator, the correlated energies are given by

$$\langle\Psi^{(0)}|\hat{H}|\Psi^{(0)}\rangle = E^{(0)} + E^{(1)} \quad \text{(A5)}$$

and

$$\frac{\langle\Psi^{(0)}+\Psi^{(1)}|\hat{H}|\Psi^{(0)}+\Psi^{(1)}\rangle}{\langle\Psi^{(0)}+\Psi^{(1)}|\Psi^{(0)}+\Psi^{(1)}\rangle} = E^{(0)} + E^{(1)} + E^{(2)} \quad \text{(A6)}$$

Here, the zeroth-order wave function $\Psi^{(0)}$ is determined by using the solvated Fock operator (i.e., in the RISM-SCF calculation). When the change of partial charges ΔQ_α is written explicitly by using the first-order wave function $\Psi^{(1)}$, the second term of eq A4 is reduced to

$$\begin{aligned}\sum_\alpha\left[\frac{\langle\Psi^{(0)}+\Psi^{(1)}|\,\hat{Q}_\alpha|\Psi^{(0)}+\Psi^{(1)}\rangle}{\langle\Psi^{(0)}+\Psi^{(1)}|\Psi^{(0)}+\Psi^{(1)}\rangle} - \langle\Psi^{(0)}|\,\hat{Q}_\alpha|\Psi^{(0)}\rangle\right]V_\alpha \\ = \frac{\langle\Psi^{(0)}+\Psi^{(1)}|\,\hat{H}-\hat{H}_0|\Psi^{(0)}+\Psi^{(1)}\rangle}{\langle\Psi^{(0)}+\Psi^{(1)}|\Psi^{(0)}+\Psi^{(1)}\rangle} - \langle\Psi^{(0)}|\,\hat{H}-\hat{H}_0|\Psi^{(0)}\rangle \\ = E^{(2)} - \frac{\langle\Psi^{(0)}+\Psi^{(1)}|\hat{H}_0|\Psi^{(0)}+\Psi^{(1)}\rangle}{\langle\Psi^{(0)}+\Psi^{(1)}|\Psi^{(0)}+\Psi^{(1)}\rangle} + \langle\Psi^{(0)}|\hat{H}_0|\Psi^{(0)}\rangle \quad \text{(A7)}\end{aligned}$$

where correlation energies given in eqs A5 and A6 are employed. In summary, the excess chemical potential $\Delta\mu$ includes correlation energy $E^{(2)}$ obtained by the MCQDPT calculation and $\Delta\mu^{\mathrm{HNC}}$ obtained by the RISM-SCF method. These terms are included in the correlated free energy defined by eq 1.

References and Notes

(1) Lippert, E.; Lüder, W.; Moll, F.; Nägele, W.; Boos, H.; Prigge, H.; Seibold-Blankenstein, I. *Angew. Chem.* **1961**, *73*, 695.

(2) Grabowski, Z. R.; Rotkiewicz, K.; Rettig, W. *Chem. Rev.* **2003**, *103*, 3899.

(3) Lippert, E.; Rettig, W.; Bonačić-Koutecký, V.; Heisel, F.; Miehé, J. A. *Adv. Chem. Phys.* **1987**, *68*, 1.

(4) Rettig, W. *Angew. Chem., Int. Ed. Engl.* **1986**, *25*, 971.

(5) Rotkiewicz, K.; Grellmann, K. H.; Grabowski, Z. R. *Chem. Phys. Lett.* **1973**, *19*, 315.

(6) Schuddeboom, W.; Jonker, S. A.; Warman, J. M.; Leinhos, U.; Kühnle, W.; Zachariasse, K. A. *J. Phys. Chem.* **1992**, *96*, 10809.

(7) Zachariasse, K. A.; Grobys, M.; von der Haar, Th.; Hebecker, A.; Il'ichev, Y. V.; Morawski, O.; Rückert, I.; Kühnle, W. *J. Photochem. Photobiol., A: Chem.* **1997**, *105*, 373.

(8) (a) Sobolewski, A. L.; Domcke, W. *Chem. Phys. Lett.* **1996**, *250*, 428. (b) Sobolewski, A. L.; Domcke, W. *Chem. Phys. Lett.* **1996**, *259*, 119.

(9) Serrano-Andrés, L.; Merchán, M.; Roos, B. O.; Lindh, R. *J. Am. Chem. Soc.* **1995**, *117*, 3189.

(10) Sobolewski, A. L.; Sudholt, W.; Domcke, W. *J. Phys. Chem. A* **1998**, *102*, 2716.

(11) Parusel, A. B. J.; Rettig, W.; Sudholt, W. *J. Phys. Chem. A* **2002**, *106*, 804.

(12) Dreyer, J.; Kummrow, A. *J. Am. Chem. Soc.* **2000**, *122*, 2577.

(13) Parusel, A. B. J.; Köhler, G.; Grimme, S. *J. Phys. Chem. A* **1998**, *102*, 6297.

(14) Parusel, A. B. J.; Köhler, G.; Nooijen, M. *J. Phys. Chem. A* **1999**, *103*, 4056.

(15) Kato, S.; Amatatsu, Y. *J. Chem. Phys.* **1990**, *92*, 7241.

(16) Hayashi, S.; Ando, K.; Kato, S. *J. Phys. Chem.* **1995**, *99*, 955.

(17) Sudholt, W.; Staib, A.; Sobolewski, A. L.; Domcke, W. *Phys. Chem. Chem. Phys.* **2000**, *2*, 4341.

(18) Gedeck, P.; Schneider, S. *J. Photochem. Photobiol., A: Chem.* **1997**, *105*, 165.

(19) Gedeck, P.; Schneider, S. *J. Photochem. Photobiol., A: Chem.* **1999**, *121*, 7.

(20) Mennucci, B.; Toniolo, A.; Tomasi, J. *J. Am. Chem. Soc.* **2000**, *122*, 10621.

(21) Cammi, R.; Mennucci, B.; Tomasi, J. *J. Phys. Chem. A* **2000**, *104*, 5631.

(22) (a) Fonseca, T.; Kim, H. J.; Hynes, J. T. *J. Mol. Liq.* **1994**, *60*, 161. (b) Fonseca, T.; Kim, H. J.; Hynes, J. T. *J. Photochem. Photobiol., A: Chem.* **1994**, *82*, 67.

(23) Kim, H. J.; Hynes, J. T. *J. Photochem. Photobiol., A: Chem.* **1997**, *105*, 337.

(24) Nordio, P. L.; Polimeno, A.; Saielli, G. *J. Photochem. Photobiol., A: Chem.* **1997**, *105*, 269.

(25) Polimeno, A.; Barbon, A.; Nordio, P. L.; Rettig, W. *J. Phys. Chem.* **1994**, *98*, 12158.

(26) Tomasi, J.; Persico, M. *Chem. Rev.* **1994**, *94*, 2027.

(27) Ten-no, S.; Hirata, F.; Kato, S. *J. Chem. Phys.* **1994**, *100*, 7443.

(28) Sato, H.; Hirata, F.; Kato, S. *J. Chem. Phys.* **1996**, *105*, 1546.

(29) Nakano, H. *J. Chem. Phys.* **1993**, *99*, 7983.

(30) Dunning, T. H., Jr.; Hey, P. J. In *Methods of Electronic Structure Theory*; Schaefer, H. F., III, Ed.; Plenum: New York, 1977.

(31) Jorgensen, W. L.; Briggs, J. M. *Mol. Phys.* **1988**, *63*, 547.

(32) Cornell, W. D.; Cieplak, P.; Bayly, C. I.; Gould, I. R.; Merz, K. M., Jr.; Ferguson, D. M.; Spellmeyer, D. C.; Fox, T.; Caldwell, J. W.; Kollman, P. A. *J. Am. Chem. Soc.* **1995**, *117*, 5179.

(33) Howard, A. E.; Cieplak, P.; Kollman, P. A. *J. Comput. Chem.* **1995**, *16*, 243.

(34) Witek, H. A.; Choe, Y.-K.; Finley, J. P.; Hirao, K. *J. Comput. Chem.* **2002**, *23*, 957.

(35) Heine, A.; Herbst-Irmer, R.; Stalke, D.; Kühnle, W.; Zachariasse, K. A. *Acta Crystallogr., Sect. B* **1994**, *50*, 363

(36) We calculated the vibrational frequencies in solution by numerical differentiations of the RISM-CASSCF gradients. The resultant zero-point energies for the ground state were 115.4 and 114.7 kcal/mol at $\tau = 0$ and 90°, respectively. These values are comparable to the gas-phase results, 114.7 and 114.0 kcal/mol, respectively. These results were also true for the LE state.

(37) Mackenzie, R. K.; MacNicol, D. D. *Chem. Commun.* **1970**, 1299.

(38) Singer, S. J.; Chandler, D. *Mol. Phys.* **1985**, *55*, 621.

(39) Chandler, D.; Singh, Y.; Richardson, D. M. *J. Chem. Phys.* **1984**, *81*, 1975.

(40) Bulliard, C.; Allan, M.; Wirtz, G.; Haselbach, E.; Zachariasse, K. A.; Detzer, N.; Grimme, S. *J. Phys. Chem. A* **1999**, *103*, 7766.

(41) Kosower, E. M.; Dodiuk, H. *J. Am. Chem. Soc.* **1976**, *98*, 924.
(42) Zachariasse, K. A.; Grobys, M.; Tauer, E. *Chem. Phys. Lett.* **1997**, *274*, 372.
(43) Changenet, P.; Plaza, P.; Martin, M. M.; Meyer, Y. H. *J. Phys. Chem. A* **1997**, *101*, 8186.
(44) (a) Okamoto, H.; Inishi, H.; Nakamura, Y.; Kohtani, S.; Nakagaki, R. *J. Phys. Chem. A* **2001**, *105*, 4182. (b) Okamoto, H. *J. Phys. Chem. A* **2000**, *104*, 4182.
(45) Hicks, J.; Vandersall, M.; Babarogic, Z.; Eisenthal, K. B. *Chem. Phys. Lett.* **1985**, *116*, 18.